Progress In Electromagnetics Research M, Vol. 116, 77–89, 2023

A Compact Reconfigurable Multi-Frequency Patch Antenna for LoRa IoT Applications

Muhammad S. Yahya[1, *], Socheatra Soeung[1], Francis E. Chinda[1], Sharul K. A. Rahim[2], Umar Musa[3], Nursyarizal B. M. Nor[1], and Cheab Sovuthy[4]

Abstract—In this study, a compact, reconfigurable, and high-efficiency Long Range (LoRa) patch antenna, which is novel, is presented for Internet of Things (IoT) applications. The antenna is designed to operate at the three major frequencies used for LoRa communication, namely 915 MHz, 868 MHz, and 433 MHz, which are widely employed for global LoRa connectivity. The compact size and impedance matching of the antenna are achieved through the use of meandered radiating patches, a partial ground plane, and a ground plane stub. The antenna is prototyped on a commercially available and cost-effective FR-4 material and measures 80 mm × 50 mm × 1.6 mm ($0.12\lambda \times 0.07\lambda$ at the lowest resonant frequency), which is smaller than the size of a standard credit card. The antenna utilizes three RF PIN diodes (SW1, SW2, and SW3) for frequency reconfiguration, which are characterized by low insertion loss and fast switching time. The RLC equivalent circuit of the antenna was validated through simulations and measurements, yielding the peak gain and radiation efficiency of 2.1 dBi and $> 90\%$, respectively. These results prove that the antenna is a promising solution for LoRa IoT applications in terms of size, cost, and performance, filling a gap in the existing literature of LoRa MPAs that are typically large, non-reconfigurable, low-gain, and single-band.

1. INTRODUCTION

LoRa is a wireless communication technology that operates in the unlicensed ISM band, providing long-range, low-power communication for IoT applications. It enables communication over long distances (more than 15 km in rural areas) and through obstacles, making it suitable for applications in smart agriculture, smart cities, industrial automation, etc. [1]. LoRa employs a method of spread-spectrum modulation known as Chirp Spread Spectrum (CSS), which allows the signal to travel farther than traditional narrowband signals by spreading the signal over a wide frequency band. In addition, LoRa utilizes a technique where the signal hops across multiple frequencies, known as FHSS (Frequency-Hopping Spread Spectrum), to mitigate interference from other devices and facilitate simultaneous data transmission and reception by multiple devices [2–5].

This combination of spread-spectrum modulation and FHSS allows LoRa to cover long distance of data transmission, typically extending several kilometers in rural areas. It also enables communication through obstacles such as buildings and trees. This feature enables the use of LoRa in a wide variety of settings, including smart cities, smart agriculture, industrial automation, logistics, supply chain, and environmental. All these capabilities make LoRa a reliable and cost-effective solution for wireless communication over long distances and in low-power devices for IoT applications.

Received 18 February 2023, Accepted 27 March 2023, Scheduled 5 April 2023
* Corresponding author: Muhammad Sani Yahya (muhammad_22000359@utp.edu.my).
[1] Universiti Teknologi PETRONAS, Seri Iskandar 32610, Malaysia. [2] Wireless Communication Centre, Universiti Teknologi Malaysia, Skudai 81310, Johor, Malaysia. [3] Faculty of Electrical and Electronic Engineering, University Tun Hussein Onn, Parit Raja, Batu Pahat 86400, Johor, Malaysia. [4] FILPAL (M) Sdn. Bhd., Bayan Lepas, Penang 11900, Malaysia

IoT on the other hand refers to a network of physical objects, such as vehicles, buildings, and devices, which have integrated electronics, software, sensors, and connectivity. These compact, low-power devices gather, process, and transmit data from multiple sources for a variety of applications, such as smart cities, industrial automation, and agriculture. IoT enhances industries by delivering valuable insights, improving operational efficiency, and fostering innovative business models [6–8].

The combination of LoRa and IoT technology is anticipated to transform various industries by providing long-range and low-power communication for IoT devices. With a growing number of IoT devices, the need for dependable, low-power communication solutions is increasing. It is expected that LoRa and IoT technology will continue to grow and evolve, with new applications and use cases being developed in the future.

Antennas play a critical role in wireless communication systems, as they are responsible for transmitting and receiving electromagnetic signals. In a LoRa wireless communication system, the antenna is responsible for providing a long-range communication link between devices. It converts the electrical signals generated by the transceiver into electromagnetic waves that can be transmitted through the air. LoRa antenna should be able to transmit and receive signals over the desired frequency band, which for LoRa is typically in the sub-gigahertz range (868 MHz, 915 MHz, or 433 MHz) depending on the region in the world.

Microstrip Patch Antenna (MPA) is a preferred choice for wireless systems due to its compact size, low profile, ease of fabrication using printed circuit board technology, wide bandwidth, low cost, good radiation pattern, and good impedance matching. These features make it easy to integrate into wireless devices and support multiple wireless standards but still cost-effective and efficient [9, 10].

A variety of antennas have been proposed for LoRa communication, including patch, dipole, and monopole antennas [11–14]. A study in [11] has introduced a new LoRa antenna designed to operate at 868 MHz for communication over water and underwater. By incorporating an oil-impregnated paper barrier around the FR-4 material antenna, the authors enhanced its bandwidth. The resulting antenna has a size of 120 mm × 70 mm × 2.4 mm and a gain of 2.11 dB. In [12], a miniaturized Planar Inverted F-shape Antenna (PIFA) designed on an FR-4 substrate for LoRa sensor node IoT applications was reported. By cutting slots on the ground plane, additional resonance was created, and the resonance frequency of the PIFA shifted down to 410 MHz from 450 MHz. The designed antenna had a realized gain of more than −6 dBi and a Voltage Standing Wave Ratio (VSWR) of less than 3, covering an overall area of 125 mm × 20 mm × 1.6 mm on the LoRa sensor node circuit board. In [13], the design, simulation, and fabrication of a multiband MPA antenna on an FR-4 substrate were presented. The antenna has a rectangular patch and three slots of different sizes at various positions to enable multiband RF energy harvesting. The antenna has achieved a peak gain of 3.94 dBi at 1585 MHz. A triangular-shaped MPA designed on an FR-4 substrate for LoRaWAN applications was presented in [14]. The antenna has a total size of 160 mm × 170 mm × 1.6 mm with a maximum gain of −5.2 dB.

These antennas have been designed for specific frequency bands, such as 868 MHz, 923 MHz, and/or 433 MHz, and have achieved good matching. However, the majority of these antennas can only operate at a single or dual LoRa bands, which limits their versatility and adaptability to changing environments. Additionally, they have a large size, low gain, low efficiency, and are non-reconfigurable which can be problematic for IoT applications that require compact and low-power devices. IoT devices are typically compact in size and require small and low-profile antennas.

Reconfigurable antennas can be employed to overcome these limitations; they can operate at multiple frequency bands. These antennas use various techniques such as switchable elements, tunable elements, and metamaterials, to achieve frequency reconfigurability [15, 16]. However, at LoRa bands (Sub 1-GHz), the realization of a compact and efficient reconfigurable MPA, which are critical requirements for IoT applications, is a very challenging task. Despite the advantages of frequency reconfigurable antennas, there is a lack of research on compact, high-efficiency, and reconfigurable LoRa patch antennas for IoT applications.

This work aims to address this gap by providing a compact, high-efficiency, and reconfigurable LoRa patch antenna that is suitable for IoT applications in major LoRa bands (915, 868, and 433 MHz). The antenna, which measures 80 mm × 50 mm × 1.6 mm ($0.12\lambda \times 0.07\lambda$ at the lowest resonant frequency) is designed and prototyped on a commercially available and cost-effective FR-4 material. It can be tuned to operate at 915 MHz, 868 MHz, and 433 MHz by strategically switching three RF PIN diodes

(SW1, SW2, and SW3) located within the radiating patches. These frequencies are widely used for LoRa communication across the globe. The compact design and impedance matching of the antenna are achieved through the use of meandered radiating patches, a partial ground plane, and a ground plane stub. As far as we know, we have not encountered any compact reconfigurable multi-frequency patch antenna capable of operating across all LoRa frequencies, which makes this work an innovative achievement.

2. METHODOLOGY

This section focuses on the techniques and procedures for designing the proposed antenna. It describes the process of designing, simulating, and testing the antenna and its various components, including the meandered radiating patches, partial ground plane, and ground plane stub. The section also covers the reconfiguration mechanisms of the antenna, including the use of RF PIN diodes for tuning the antenna to different frequencies.

2.1. Theory and Structure of the Antenna

The geometrical property of the proposed antenna is depicted in Fig. 1. Meandered patch lines are employed on the upper surface of an FR-4 substrate that is 1.6 mm in thickness with $\varepsilon_r = 4.4$ and $\tan\delta = 0.02$ and a partial ground plane on the bottom side. The meandered lines determined using the theory of transmission line modelling [17] are folded to achieve the desired resonant frequencies at 915 MHz, 868 MHz, and 433 MHz depending on the state of switches SW1, SW2, SW3. To improve matching at 433 MHz, a stub ($L_{Stub} \times W_{Stub}$) is placed above the partial ground plane as presented in Fig. 1(b). Silicon PIN diodes (BAR50-02V) from Infineon are used as SW1, SW2, and SW3 due to their fast-switching time and low insertion loss. These PIN diodes together with their bias circuits are soldered atop of the substrate shown in Fig. 1(a). The details of these switches are presented in Fig. 1(c). The schematics of the equivalent circuitries of the PIN diodes in ON and OFF and their biasing circuits are presented in Fig. 2. The DC blocking capacitors in the biasing circuit are placed strategically to prevent the DC biasing voltage from entering the RF source. The standard dimensions of 80 mm × 50 mm which is less than the size of a standard credit card are chosen to achieve compactness of the antenna for integration with emerging IoT devices. The substrate is chosen for its low cost and wide availability. Compact antennas with dimensions like a credit card size would be portable, save

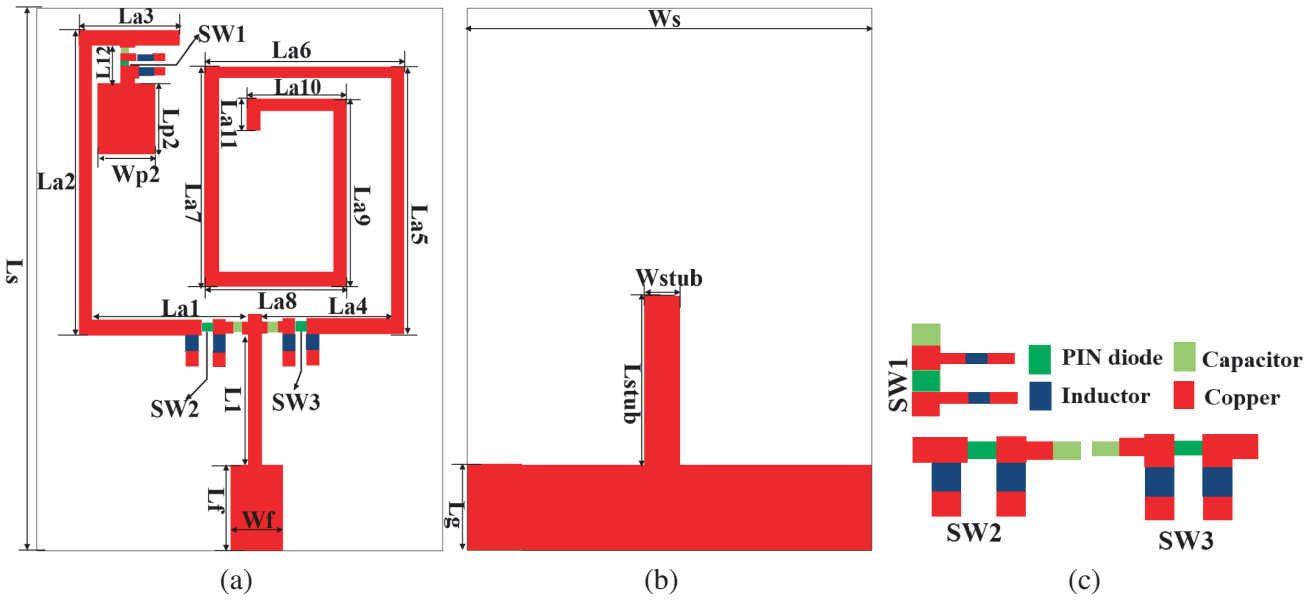

Figure 1. (a) Geometry of the proposed antenna. (a) Front. (b) Back. (c) Details of the switches.

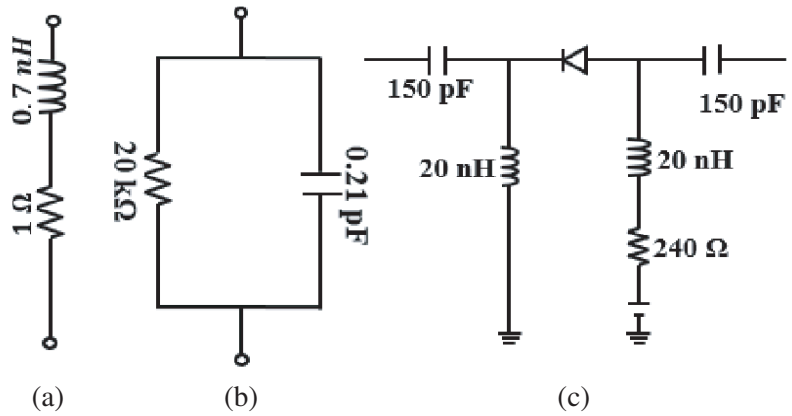

Figure 2. Equivalent circuit of RF PIN Diode. (a) ON. (b) OFF. (c) Biasing circuit.

Table 1. Specifications of the dimensions of the antenna.

Parameter	Dimensions (mm)	Parameter	Dimensions (mm)	Parameter	Dimensions (mm)	Parameter	Dimensions (mm)
L_s	80	W_s	50	L_f	13	W_f	8
L_1	21	WL_1	2	La_1	23	WLa_1	2
La_2	45	WLa_2	2	La_3	11.7	WLa_3	2
La_4	23	WLa_4	2	La_5	41	WLa_5	2
La_6	32	WLa_6	2	La_7	35	WLa_7	2
La_8	22.5	WLa_8	3	La_9	30	WLa_9	2
La_{10}	16	WLa_{10}	2	La_{11}	3	WLa_{11}	2
L_{12}	3	WL_{12}	3	Wp_2	8.5	Lp_2	12
L_{stub}	24	W_{stub}	2.5	L_g	13	W_g	50

space, and cost-effective for LoRa systems. CST MWS is used for the design, tuning, and analysis of the antenna. The antenna is excited via a 50 Ω microstrip feed line with a dimension $L_f \times W_f$. The detailed dimensions of the proposed design are given in Table 1.

2.2. Reconfiguration Mechanism of the Antenna

The reconfiguration mechanism of the proposed antenna is a critical aspect of the design, which enables the antenna to operate at three distinct frequencies: 915 MHz, 433 MHz, 868 MHz. The purpose of this section is to discuss the theoretical principles behind the reconfiguration mechanism, the PIN diode/switch modelling in CST MWS, and the practical aspects of the biasing circuit. The proposed antenna is reconfigured through the use of three PIN diodes, SW1, SW2, and SW3, serving as switches. The frequency of operation of the antenna is dependent upon the state of the diodes, which can either be ON or OFF. This results in an adjustment of the length of the meandered radiating structure, leading to the desired frequency tuning. The resonant frequency of a patch antenna is directly related to its physical length and can be adjusted by changing the effective electrical length of the patch. When both SW1 and SW2 are OFF, and SW3 is ON, the antenna operates at 433 MHz and 915 MHz. When SW1 is OFF, SW2 ON, and SW3 OFF, the antenna operates at 915 MHz. On the other hand, when both SW1 and SW2 are ON, and SW3 is OFF, the antenna operates at 868 MHz. To ensure the reconfigurability of the proposed antenna and its ability to tune to the desired frequencies, the values of the ON and OFF equivalent circuit parameters are appropriately selected from the data sheet of the diode. When the diode is in the ON state, it exhibits low impedance behavior, whereas in the OFF state, it behaves as

a high impedance connection. The ON and OFF equivalent circuits for PIN diode are shown in Fig. 2.

In the simulation, CST MWS software is used to model and simulate the behavior of the PIN diode in both its ON and OFF states. The software uses the equivalent circuit parameters, such as resistance, reactance, and capacitance, to model the behavior of the diode in both the ON and OFF states. When the diode is in the ON state, it exhibits low impedance behavior, and the simulation shows this by using the low resistance value in the equivalent circuit representation. Conversely, when the diode is in the OFF state, it acts as a high impedance connection, and the simulation represents this by using the high resistance value in the equivalent circuit.

3. RESULTS AND ANALYSIS

To evaluate the performance of the proposed antenna, some critical performance metrices such as Voltage Standing Wave Ratio (VSWR), gain, directivity, far field patterns, return loss (S_{11}), and surface currents would be studied. The results of these metrices provide a comprehensive understanding of the behavior of the proposed design and its ability to tune to the desired frequencies of 915 MHz, 433 MHz, and 868 MHz as determined by the state of the PIN diodes, SW1, SW2, and SW3, used as switches. The fabricated prototype of the antenna is depicted in Fig. 3.

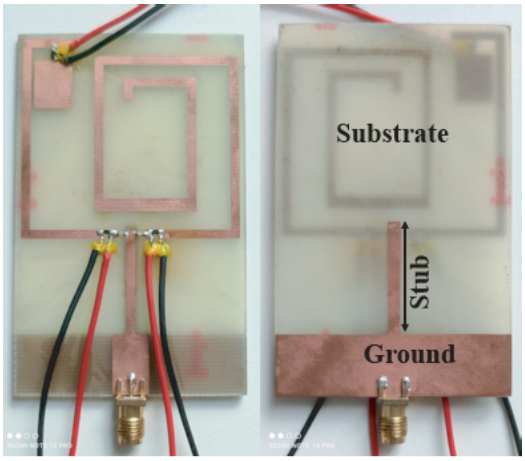

(a) (b)

Figure 3. Prototype antenna. (a) Front. (b) Back.

S_{11}, also known as reflection loss, is a crucial performance metric in antenna design and analysis. It denotes the magnitude of the reflected power resulting from an impedance mismatch in the transmission line. A high S_{11} indicates a well-matched system with low reflection, whereas a low S_{11} signifies a poorly matched system with high reflection. The measurement of S_{11} is an important step in ensuring the reliability and stability of an antenna. In this section, the results of the S_{11} simulation and measurement of the proposed antenna and its analysis are presented. The results of the comparison between the simulation and measurement of the S_{11} for the proposed antenna with SW1 and SW2 OFF and SW3 ON are depicted in Fig. 4. This configuration results in a dual band operation at 433 MHz and 915 MHz. The measured S_{11} of the antenna is found to be more than -25 dB and -30 dB at 433 MHz and 915 MHz, respectively.

Similarly, Fig. 5 depicts the comparison between simulation and measurement results of the antenna with SW1 and SW2 ON and SW3 OFF configuration. It shows a resonant frequency at 868 MHz with measured S_{11} of -19 dB.

Furthermore, Fig. 6 shows the comparison between simulation and measurement results of the antenna with SW1 OFF, SW2 ON, and SW3 OFF configuration. A measured S_{11} greater than -30 dB is observed.

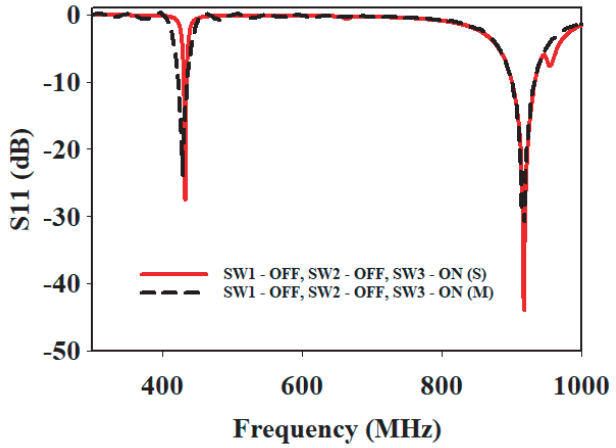

Figure 4. S_{11} at 433 MHz and 915 MHz.

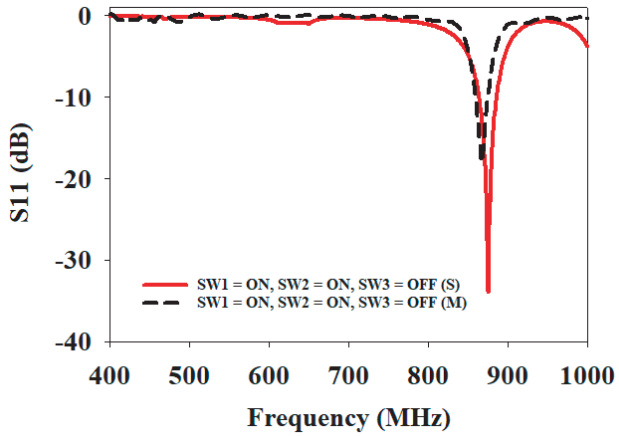

Figure 5. S_{11} at 868 MHz.

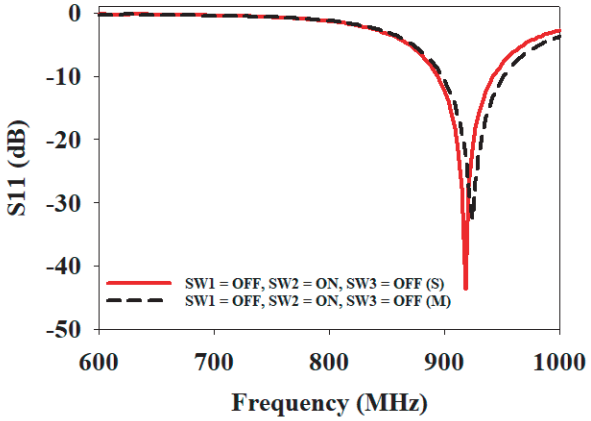

Figure 6. S_{11} at 915 MHz.

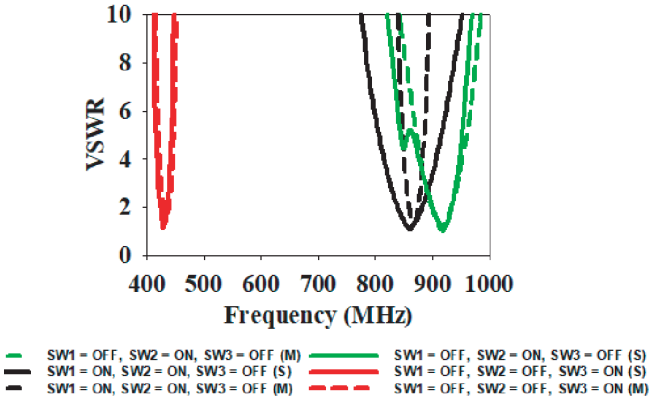

Figure 7. VSWR of the antenna at different switching states.

It can be noted that in each case the simulation and measurement results of the antenna exhibit low levels of S_{11}. A low S_{11} value indicates that most of the input power has been transmitted, rather than being reflected back to the source.

3.1. VSWR

VSWR is an important parameter used to evaluate the performance of an antenna. It is a measure of the mismatch between the antenna and transmission line and indicates the degree to which the radio waves are reflected back to the source. A low VSWR value indicates that the majority of the radio waves are transmitted, while a high VSWR value indicates that there is a significant amount of reflected power, causing loss and degradation of the signal. In this subsection, the VSWR of the proposed antenna will be discussed and analyzed. The VSWR results from simulations and measurements will be compared to determine the effectiveness of the antenna in transmitting the radio waves. The results depicted in Fig. 7 reveal that the proposed antenna has excellent impedance matching performance in all of its modes of operation. A VSWR of less than 2 indicates that the reflected power is minimal, thereby allowing for efficient transfer of power from the transmission line to the radiating space. This desirable characteristic highlights the ability of the antenna to deliver high-quality signals in all of its modes.

3.2. Current Distribution

A comprehensive understanding of the antenna's operation requires an examination of the current distributions associated with its different switching states. The current distributions on the antenna, in response to the configurations of SW1, SW2, and SW3, are displayed in Fig. 8 and Fig. 9. By analyzing the current distributions, key information about the performance and mode-specific operation of the antenna can be gathered. The pattern of current distribution plays a significant role in determining the radiation characteristics and impedance matching of the antenna.

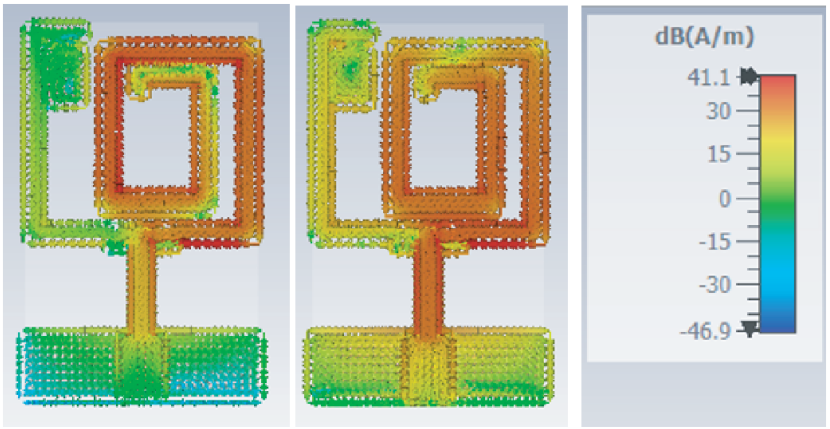

(a) (b)

Figure 8. Current distribution. (a) 433 MHz. (b) 915 MHz.

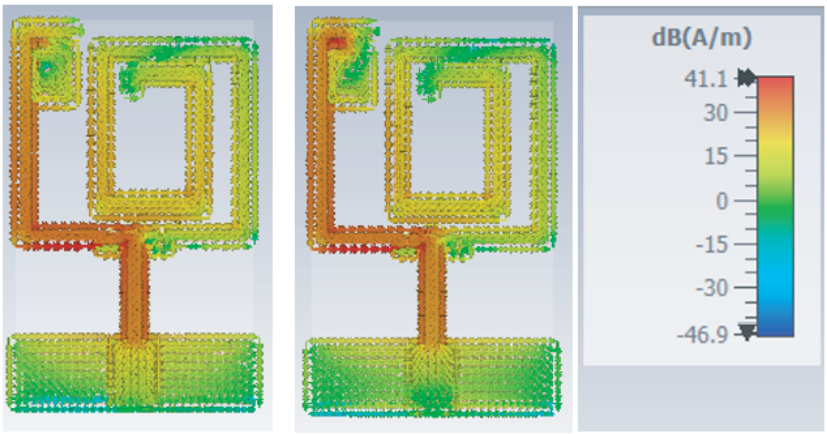

(a) (b)

Figure 9. Current distribution. (a) 915 MHz. (b) 868 MHz.

The section of the patch that is responsible for the dual-band operation at 433 MHz and 915 MHz, when SW1 = OFF, SW2 = OFF, and SW3 = ON, is presented in Fig. 8. A visual examination of Fig. 8(a) reveals that La4, La5, La6, La7, La8, and the edges of La9, La10, and La11 have the highest current density, as indicated by the red color in the current distribution plot. This produced the resonance at 433 MHz. Similarly, La4, La5, La7, La8, La9, La10, La11, and the edges of La6 produced the resonance at 915 MHz as shown in Fig. 8(b). This result highlights the crucial role played by these specific regions of the patch in achieving dual band operation and provides important insights into the mechanism of the antenna's operation in this mode.

On the other hand, when SW1 is set to OFF, SW2 set to ON, and SW3 set to OFF, the current distribution in the antenna shows maximum density in the elements La1 and La2 as depicted in Fig. 9(a). This indicates that these elements are primarily responsible for producing the resonance frequency of 915 MHz in the antenna. This current distribution is determined by the positions and settings of the switches, which control the flow of current in different elements of the antenna. The particular configuration of the switches in this case results in maximum current flowing through La1 and La2, causing them to produce the required resonant frequency. In contrast, when the switch configuration is set to SW1 = ON, SW2 = ON, and SW3 = OFF, the antenna exhibits a current distribution pattern with peak current densities in La1, La2, and a portion of La3. These elements as shown in Fig. 9(b) collectively contribute to the generation of the 868 MHz resonant frequency in the antenna. The switch configuration plays a crucial role in directing the flow of current through the various components of the antenna. This results in selective excitation of the desired resonant mode in La1, La2, and part of La3. The tunability of the resonant frequency can be achieved by modulating the switch configuration to adjust the current distribution in the antenna.

3.3. Radiation Pattern

In this subsection, a comprehensive analysis of the radiation pattern of the proposed antenna at different switching states is presented. The focus will be on comparing the simulation results with the experimental measurements. This comparison will provide insight into the accuracy of the simulation model to assess the functionality of the antenna.

The results of the radiation pattern analysis for different configurations of the switches are presented in Fig. 10. Fig. 10(a) depicts the E-plane and H-plane radiation patterns when both SW1 and SW2 are turned OFF, and SW3 is turned ON. Fig. 10(b) presents the comparison between simulated and measured azimuth and elevation plane radiation patterns when both SW1 and SW2 are turned ON, and SW3 is turned OFF. Additionally, the plot in Fig. 10(c) represents the comparison between simulated and measured H-plane and E-plane radiation patterns when SW1 is turned OFF, SW2 turned ON, and SW3 turned OFF. It is evident from each mode that the antenna demonstrates an omnidirectional H-plane radiation pattern, which indicates that the antenna radiates uniformly in the azimuthal direction. However, the E-plane radiation pattern exhibits a bi-directional nature, which means that the antenna radiates in two opposite directions along the elevation plane.

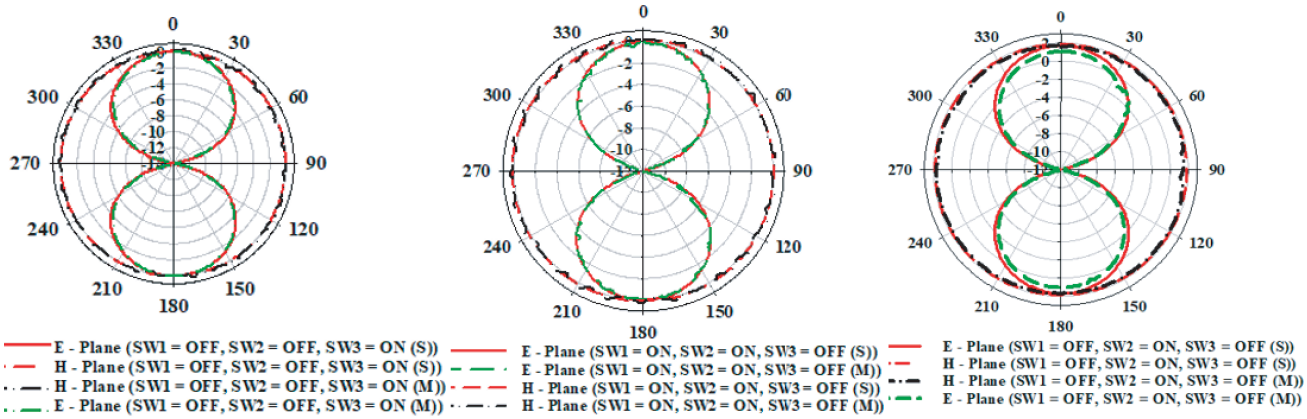

(a) (b) (c)

Figure 10. Radiation pattern. (a) 433 MHz and 915 MHz. (b) 868 MHz (c) 915 MHz.

In the case of a LoRa patch antenna, an omnidirectional H-plane radiation pattern is desirable as it ensures that the antenna can communicate effectively with devices in all directions. The bi-directional E-plane radiation pattern implies that the antenna will have a certain degree of directional gain, which can be beneficial in increasing the communication range.

It is noteworthy that both simulation and measurement results are in good agreement, which implies that the simulation model accurately predicts the radiation behavior of the antenna.

3.4. Gain and Efficiency

The performances of the antenna's gain and efficiency are presented in Fig. 11 and Fig. 12. Fig. 11 shows the comparison of the measured and simulated gains of the antenna at 433 MHz, where a measured gain of 1.94 dBi is observed. Fig. 12 depicts the comparison of the measured and simulated gains of the antenna at 868 MHz and 915 MHz, respectively, which are 2.01 dBi and 2.1 dBi. The results indicate that the antenna has good performance in terms of gain across all the frequency bands. Additionally, the efficiency of the antenna is found to be above 90% in each band of operation, indicating that most of the input power is effectively radiated into free space. The slight difference between the simulated and measured values can be attributed to the inherent inaccuracies in the simulation model and measurement equipment. Nevertheless, the difference is within acceptable limits, and the results can be considered to be in good agreement.

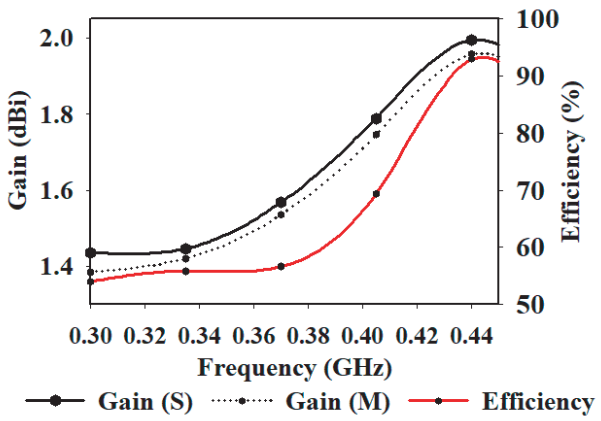

Figure 11. Gain and efficiency of the antenna at 433 MHz.

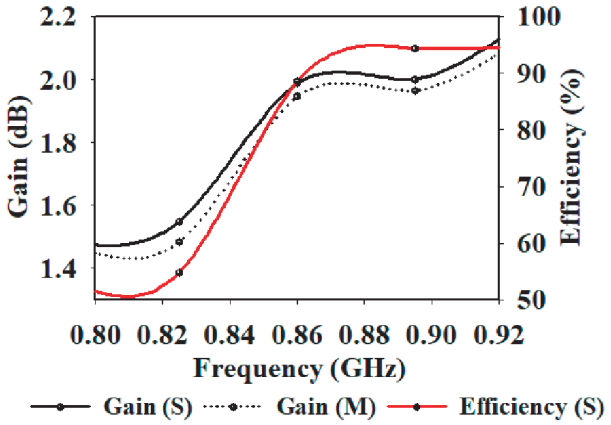

Figure 12. Gain and efficiency of the antenna at 868 MHz and 915 MHz.

4. RLC EQUIVALENT CIRCUIT MODELS

The RLC equivalent circuit model is a widely used lumped-element model for the analysis and simulation of RF and microwave circuits and antennas. The model is based on the equivalent representation of an antenna using passive elements, such as resistors, inductors, and capacitors, to capture its electrical behavior. The RLC model provides a simple and computationally efficient method for modelling the behavior of an antenna. A rectangular MPA can be mathematically represented as a parallel combination of a Resistor (R), Inductor (L), and Capacitor (C).

This electrical equivalent circuit model of the MPA is based on the cavity model, which assumes that the patch antenna can be modelled as a resonant cavity with the patch acting as the top plate and the ground plane as the bottom plate.

The resistor (R) in the equivalent circuit represents the losses in the metal of the patch antenna, such as the resistance of the metal and the skin effect. The inductor (L) represents the inductive reactance of the patch antenna, which is related to the resonant frequency of the cavity. The capacitor (C) represents the capacitive reactance of the patch antenna, which is related to the storage of energy in the cavity.

These RLC components can be used to predict the electromagnetic behavior of the MPA, such as its resonant frequency, impedance, and radiation patterns. The values of R, L, and C can be calculated using mathematical equations based on the dimensions and materials of the MPA. This equivalent circuit model provides a simple and effective way to analyze and design microstrip patch antennas. Considering the physical structure of the proposed antenna with respect to different configurations of the switches, the RLC values are determined from Equations (1)–(4) based on the approach presented

in [18].

$$C_1 = \frac{\varepsilon_e \varepsilon_o L_1 W_1}{2h} F \tag{1}$$

$$L_1 = \frac{1}{(2f_r)^2} C_1 \tag{2}$$

$$R_1 = \frac{Q_r}{2 f_r C_1} \tag{3}$$

$$F = \cos^{-2}\left(\frac{\pi^2 y_o}{L}\right) \tag{4}$$

y_o = the distance from the excitation point to the patch, ε_r = dielectric constant of the substrate, ε_o = free space permittivity, L_1 = length of the patch, W_1 = width of the patch, f_r = operating frequency of the element

The Advanced Digital System (ADS) software is used to model, simulate, optimize, and tune the RLC antennas to achieve desired resonance based on different switch configurations. Fig. 13 to Fig. 18 illustrate the RLC equivalent circuit models of the antenna and their corresponding S_{11} plots for different switch states. In Fig. 13, the RLC equivalent circuit model of the antenna with SW1 OFF, SW2 OFF, and SW3 ON is depicted. The S_{11} plot of the antenna shown in Fig. 14 indicates dual bands at 433 MHz and 915 MHz with a magnitude greater than −20 dB in each band. On the other hand, the RLC equivalent circuit model of the antenna with the configurations of SW1 ON, SW2 ON, and SW3 OFF is depicted in Fig. 15. The antenna has achieved an S_{11} greater than −20 dB at 868 MHz based on the plot of S_{11} presented in Fig. 16. Additionally, the RLC equivalent circuit model of the antenna when SW1 is OFF, SW2 ON, and SW3 OFF is shown in Fig. 17. It is evident from Fig. 18 that the antenna has an S_{11} greater than −20 dB at 915 MHz.

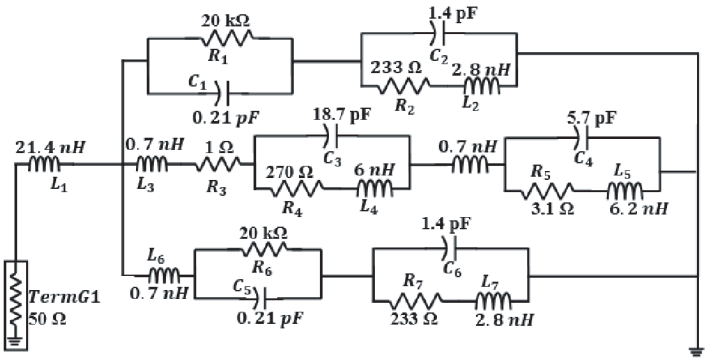

Figure 13. RLC equivalent circuit model at 433 MHz and 915 MHz.

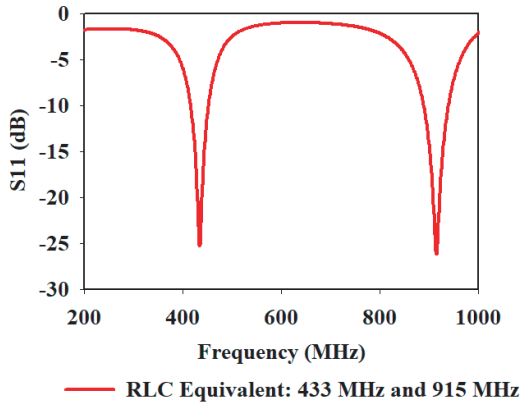

Figure 14. S_{11} at 433 MHz and 915 MHz.

Therefore, the RLC equivalent circuit model is crucial for validating antenna simulation and measurement results. It allows for the quick and accurate verification of antenna performance and provides valuable insights into its behavior. The model can also be easily optimized and refined based on measured data, leading to improved simulation accuracy. However, it should be noted that many antenna designers do not give adequate attention to RLC equivalent circuit models, which is essential for accurate antenna design.

The comparison between the proposed antenna and existing literature is presented in Table 2. The results show that the proposed antenna stands out as a unique design with its compact size, multiband capabilities, and reconfigurable features. This is in stark contrast to existing LoRa MPA antennas which are typically large in size, non-reconfigurable, low in gain, and operate in a single band. Moreover, the proposed antenna exhibits improved performance compared to existing literature.

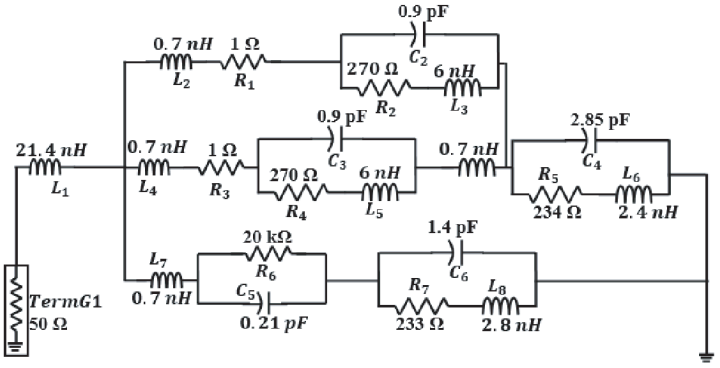

Figure 15. RLC equivalent circuit model at 868 MHz.

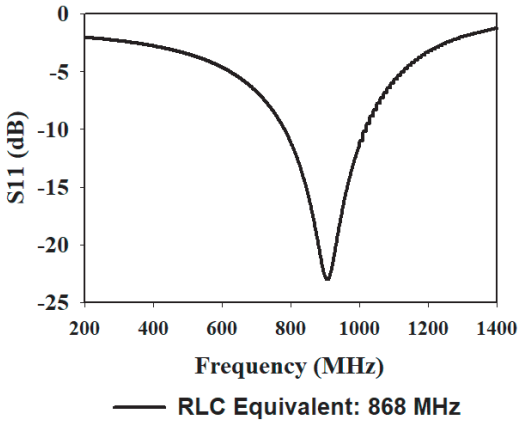

Figure 16. S_{11} at 868 MHz.

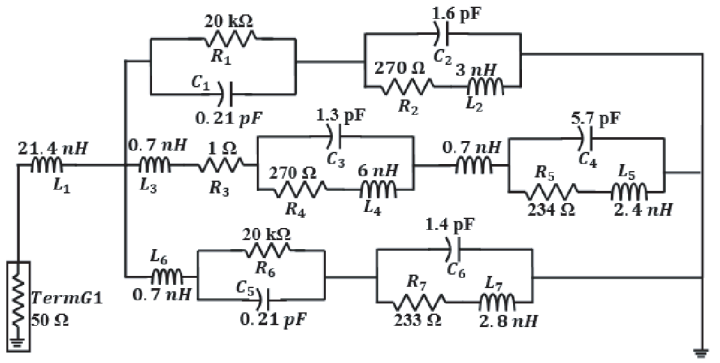

Figure 17. RLC equivalent circuit model at 915 MHz.

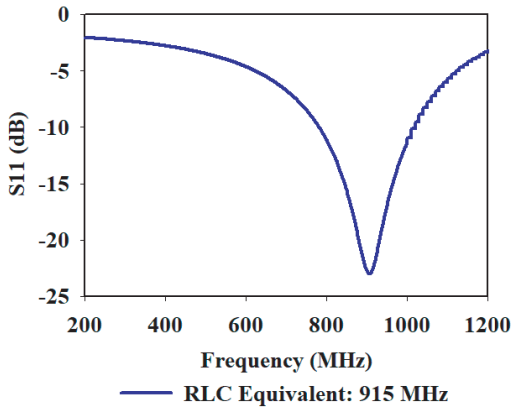

Figure 18. S_{11} at 915 MHz.

Table 2. Comparison of the performance of the proposed antenna with available literatures.

Ref.	Year	Bands	Freq. (MHz)	Substrate	Conductive material	Gain (dBi)	Reconfi-gurable?	All LoRa Freq?	Size (mm^2)
[11]	2021	1	868	FR-4 ($\varepsilon_r = 4.3$)	Copper	2.11	NO	YES	$0.35\lambda \times 0.20\lambda$
[12]	2018	1	402.4–441.6	FR-4 (NA)	Copper	−6	NO	YES	$0.18\lambda \times 0.03\lambda$
[13]	2020	4	865–880 1525–1605 1790–1868 2085–2125	FR-4 (4.4)	Copper	1.29 dBi at 867.7 MHz 3.94 dBi at 1585.5 MHz 1.15 dBi at 1801.9 MHz 0.89 dBi at 2095.8 MHz	NO	NO	$0.24\lambda \times 0.13\lambda$
[14]	2021	2	400 900.2	FR-4 (NA)	Copper	−5 dB	NO	YES	$0.23\lambda \times 0.25\lambda$
This work		**3**	**433** **868** **915**	**FR-4 (4.4)**	**Copper**	**1.98 dBi at 433 MHz** **2.01 dBi at 868 MHz** **2.1 dBi at 915 MHz**	**YES**	**YES**	$\mathbf{0.12\lambda \times 0.07\lambda}$

The superiority of the proposed antenna over existing LoRa MPAs can be attributed to its innovative design and advanced capabilities. The compact size, multiband capability, and reconfigurable features of the proposed antenna make it a suitable option for LoRa IoT applications, whereas previously reported LoRa patch antennas are not suitable for these applications due to their limited capabilities.

It is important to note that LoRa IoT applications demand efficient and reliable communication devices. The limitations of existing LoRa patch antennas, such as large size, non-reconfigurable, low gain, and single band operation, make them unsuitable for these applications. In contrast, the proposed antenna, with its compact size, multiband capability, and reconfigurable features, demonstrates its potential as a suitable solution for LoRa IoT applications.

The comparison in Table 2 highlights the innovative aspects of the proposed antenna and demonstrates its superiority in terms of its design and performance compared to existing LoRa MPAs. The compact, multiband, and reconfigurable features of the proposed antenna set it apart from other existing designs, making it a valuable contribution to the field. Additionally, the comparatively good performance of the proposed antenna further supports its effectiveness and viability for practical applications.

5. CONCLUSION

In this paper, a novel compact frequency reconfigurable triple-band antenna for LoRa IoT applications was reported. The antenna utilizes three RF PIN diodes to switch among three different frequency bands: 433 MHz, 868 MHz, and 915 MHz, which are used for LoRa in different regions such as Europe, America, and Asia. This design is cost-effective and miniaturized ($0.12\lambda \times 0.07\lambda$ at the lowest resonant frequency), making it a practical solution for LoRa IoT applications. The RLC equivalent circuit of the antenna was compared with simulation and measurement results, demonstrating its exceptional performance with a peak gain of 2.1 dBi and a radiation efficiency above 90%. The antenna was also prototyped and tested, yielding results that were in good agreement with simulations. These findings suggest that the proposed antenna is a promising solution for LoRa IoT applications in terms of size, cost, and performance.

ACKNOWLEDGMENT

We would like to express our heartfelt gratitude to the Petroleum Technology Development Fund (PTDF) Nigeria and Universiti Teknologi PETRONAS (UTP) Malaysia for their unwavering support in making this research a reality.

REFERENCES

1. Ayoub Kamal, M., M. M. Alam, A. A. Sajak, and M. Mohd Su'ud, "Requirements, deployments, and challenges of LoRa technology: A survey," *Comput. Intell. Neurosci.*, 2023.
2. Edward, P., M. El-Aasser, M. Ashour, and T. Elshabrawy, "Interleaved chirp spreading LoRa as a parallel network to enhance LoRa capacity," *IEEE Internet Things J.*, Vol. 8, No. 5, 2020.
3. Edward, P., S. Elzeiny, M. Ashour, and T. Elshabrawy, "On the coexistence of LoRa-and interleaved chirp spreading LoRa-based modulations," *2019 International Conference on Wireless and Mobile Computing, Networking and Communications (WiMob)*, 2019.
4. Opipah, S., H. Qodim, D. Miharja, E. A. Z. Hamidi, and T. Juhana, "Prototype design of smart home system base on LoRa," *2020 6th International Conference on Wireless and Telematics (ICWT)*, 2020.
5. El-Aasser, M., A. Gasser, M. Ashour, and T. Elshabrawy, "Performance analysis comparison between LoRA and frequency hopping-based LPWAN," *2019 IEEE Global Conference on Internet of Things (GCIoT)*, 2019.
6. Munirathinam, S., "Industry 4.0: Industrial Internet of Things (IIOT)," *Advance in Computers*, Vol. 117, No. 1, 129–164, 2020.

7. Swamy, S. N. and S. R. Kota, "An empirical study on system level aspects of Internet of Things (IoT)," *IEEE Access*, Vol. 8, 188082–188134, 2020.
8. Chaudhary, S., R. Johari, R. Bhatia, K. Gupta, and Bhatnagar, "CRAIoT: Concept, review and application(s) of IoT," *2019 4th International Conference on Internet of Things: Smart Innovation and Usages (IoT-SIU)*, 2019.
9. Masuk, A., O. M. Kende, A. Husam, and I. Balajti, "Cyber-physical system aspects of microstrip patch antenna of radar sensor application," *2022 23rd International Radar Symposium (IRS)*, 2022.
10. Moradi, A. and T. B. A. Rahman, "Broadband modified rectangular microstrip patch antenna using stepped cut at four corners method," *Progress In Electromagnetics Research*, 599–619, 2013.
11. Dala, A. and T. Arslan, "Design, implementation, and measurement procedure of underwater and water surface antenna for Lora communication," *Sensors*, Vol. 21, No. 4, 1337, 2021.
12. Zhang, Q. and Y. Gao, "Embedded antenna design on LoRa radio for IoT applications," *12th European Conference on Antennas and Propagation*, London, UK, Apr. 2018.
13. Boursianis, A. D., M. S. Papadopoulou, J. Pierezan, V. C. Mariani, L. S. Coelho, P. Sarigiannidis, S. Koulouridis, and S. K. Goudos, "Multiband patch antenna design using nature-inspired optimization method," *IEEE Open Journal of Antennas and Propagation*, 151–162, 2020.
14. Krishna, M. V. and G. S. N. Raju, "Triangle shaped antenna design for IoT-based Lorawan applications," *SAMRIDDHI: A Journal of Physical Sciences, Engineering and Technology*, Vol. 13, No. 01, 8–11, 2021.
15. Musa, U., S. M. Shah, H. A. Majid, Z. Z. Abidin, M. S. Yahya, S. Babani, and Z. Yunusa, "Recent advancement of wearable reconfigurable antenna technologies: A review," *IEEE Access*, Vol. 10, 121831–121863, 2022.
16. Pourziad, A., S. Nikmehr, and H. Veladi, "A novel multi-state integrated RF MEMS switch for reconfigurable antennas applications," *Progress In Electromagnetics Research*, Vol. 139, 389–406, 2013.
17. Ullah, S., S. Ahmad, and B. A. Khan, "A multi-band switchable antenna for Wi-Fi, 3G advanced, WiMAX, and WLAN wireless applications," *International Journal of Microwave and Wireless Technologies*, Vol. 10, No. 8, 991–997, 2018.
18. Awaleh, A. A., S. H. Dahlan, and M. Z. M. Jenu, "Equivalent electrical lumped component modeling of e-shaped patch flat lens antenna unit cell," *In 2014 IEEE Asia-Pacific Conference on Applied Electromagnetics (APACE)*, 2014.